



HAL
open science

Crashworthiness of poplar wood veneer tubes

R. Guélou, Florent Eyma, Arthur Cantarel, Samuel Rivallant, Bruno Castanié

► **To cite this version:**

R. Guélou, Florent Eyma, Arthur Cantarel, Samuel Rivallant, Bruno Castanié. Crashworthiness of poplar wood veneer tubes. *International Journal of Impact Engineering*, 2021, 147, pp.103738. 10.1016/j.ijimpeng.2020.103738 . hal-02975947

HAL Id: hal-02975947

<https://insa-toulouse.hal.science/hal-02975947v1>

Submitted on 23 Oct 2020

HAL is a multi-disciplinary open access archive for the deposit and dissemination of scientific research documents, whether they are published or not. The documents may come from teaching and research institutions in France or abroad, or from public or private research centers.

L'archive ouverte pluridisciplinaire **HAL**, est destinée au dépôt et à la diffusion de documents scientifiques de niveau recherche, publiés ou non, émanant des établissements d'enseignement et de recherche français ou étrangers, des laboratoires publics ou privés.

Crashworthiness of poplar wood veneer tubes

R. Guélou^a, F. Eyma^a, A. Cantarel^a, S. Rivallant^a, B. Castanié^{a,*}

^aInstitut Clément Ader (ICA), ISAE, CNRS UMR 5312-INSA-Mines Albi-UPS, Toulouse, France

* Corresponding author: bruno.castanie@insa-toulouse.fr

Keywords: Wood, Poplar, Crushing, Energy absorption, Static, Dynamic

Abstract

This work studies the potential of using wooden tubes for crash applications. The tubes were made from 1 mm thick “l214” poplar veneers, according to different stacking sequences. Four configurations were characterized under static crushing (5 mm/min) and the one that performed best ((90/0₄/90)) was chosen to undergo dynamic tests under a drop weight tower (5.7 m/s). This configuration presents significant energy absorption performance in static (31.6 J / g) and in dynamic (28.5 J / g) crushing for a material that is natural, ecological (low carbon footprint), recyclable, and low cost in comparison with other materials such as composite materials. As with composites, the position, number, and orientation of the plies directly affect the amount of energy absorbed. The use of poplar, one of the weakest woods in mechanical terms, shows the possibilities of wood for this use.

1. Introduction

Wood, by its nature, is an ecological material that has a very low grey energy (energy required from the creation of the raw material to the installation of the finished product) due, in particular, to its capacity to store carbon [1, 2]. It is also a recyclable material that, once it reaches the end of its life, can be used for the manufacture of particle boards or for energy recovery (heating). Additionally, it is, a material that is much cheaper than others. Wood or plywood are generally used in construction and furniture but also

26 have applications in other fields, such as civil light aviation, boating, and the nuclear industry or, in the
27 past, the automobile industry [3- 6]. Plywood has good **weight** specific mechanical properties under
28 bending, tension, compression and shear [7].

29 There are few studies on the impact or crash behaviour of wood. Johnson analysed the problem in 1986,
30 mainly from a historical point of view in the naval field [8]. Some studies have been carried out to study
31 the dynamic behaviour of wood via tests on Hopkinson bars [9-12] but few dynamic studies have been
32 carried out on drop weight apparatus. **Adalian and Morlier** [13], however, studied the behaviour, in the
33 longitudinal and tangential directions, of poplar in the form of massive rectangular specimens with this
34 kind of tests. The objective of their study was to obtain enough static and dynamic compression data to
35 be able to model wood as a shock absorber. The force-displacement curve showed that the dynamic
36 performance of poplar was slightly better than its static performance in the longitudinal or tangential
37 direction (Plateau force, Energy Absorbed (EA) or Specific Energy Absorbed (SEA)). There is now
38 renewed interest in these materials and the issue [15-18]. **Some very interesting studies have also been**
39 **conducted on the dynamic behaviour of coconut woods [19-21].**

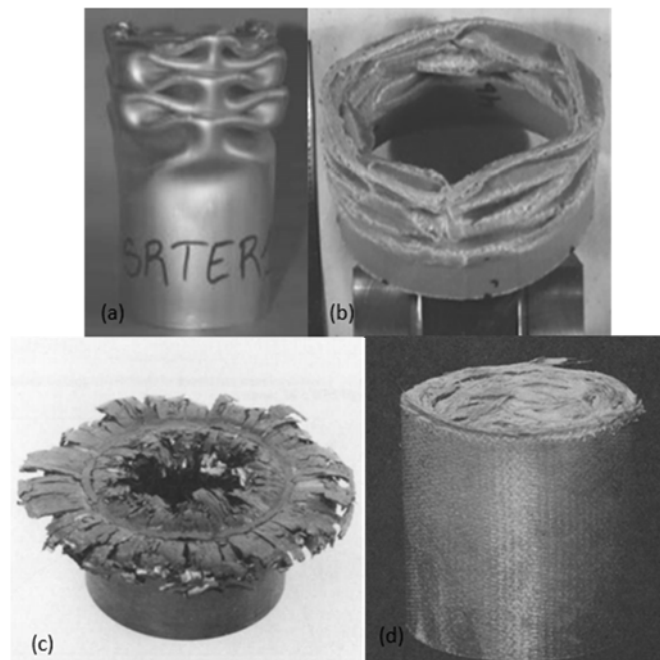
40 Susainathan et al. studied various configurations of sandwich plates with composite skins (aluminium,
41 carbon, glass, and flax) and a plywood core subjected to low speed / low energy impacts [16]. They
42 demonstrated that, as a core material, it was better to have a plywood that multiplies the interfaces (i.e.
43 the number of plies) to improve the transverse behaviour and thus the impact response. These authors
44 also investigated the numerical modelling of this type of impact in a preliminary manner, but this is a new
45 field requiring a very great amount of characterization work [17]. It can therefore be argued that
46 experimental studies on these types of materials should be done first. Then the same authors tested
47 sandwiches and plywood alone in compression and compression after impact [18]. The two plywoods,
48 alone or sandwiched with aluminium, flax or glass skins, showed a remarkable response in compression
49 after impact of the panels with, in particular, the presence of a plateau on the force-displacement curve

50 and a high residual resistance. Because of these good characteristics of plywood after impact and
51 compression, the question arises as to the use of these structures for crash applications.

52 Given the small number of studies for wood, it is wise to focus on composite materials, which will serve
53 as a reference for this study because their use has increased significantly in recent years despite their
54 complexity [22]. In the crash domain, the low density and high specific resistances of composite materials
55 make it possible to obtain very interesting energy absorption when they are appropriate to the failure
56 mode [23-34]. The energy absorption potential of a material is assessed using the SEA (Specific Energy
57 Absorption, which corresponds to the energy absorbed per unit of mass). The different configurations and
58 numerous parameters that vary among the studies available in the literature generate a wide range of
59 SEA for composite materials. Guillon [23] showed that, for carbon-epoxy plates, the SEA varied according
60 to the main mode of damage. A pure splaying mode generated a low SEA, between 4 and 7 J/g. The SEA
61 was from 33 to 50 J/g for a failure mode with predominant fragmentation, and from 10 to 15 J/g in the
62 case of a combination of these two modes (known as brittle fracture mode). For circular carbon-epoxy
63 tubes with an internal diameter of 50 mm oriented at $\pm 15^\circ$, Wang et al. [26] obtained a SEA of 94 J/g,
64 and a SEA of 73 J/g for an orientation of $\pm 45^\circ$. Hamada et al. [27], also on circular carbon tubes with an
65 internal diameter of 50 mm [$\pm 45^\circ$], found a SEA of 53 J/g. When the carbon fibres were combined with
66 a PEEK resin, a significant improvement was observed, with a SEA of 180 J/g. Glass fibres have
67 interesting SEA, and Hu et al. [28] obtained 77 J/g on 50 mm diameter circular tubes oriented at $\pm 15^\circ$.

68 With glass fibre tubes 55 mm in internal diameter, Song [29] reached 50 to 60 J/g depending on the
69 trigger, with fibres oriented at [$\pm 45^\circ$] and in local buckling mode. Yan and Chouw [30] obtained an optimal
70 configuration reaching 42 J/g on circular tubes with an internal diameter of 36 mm, made of flax fibres
71 with [0/90] stacking. For tubes, the failure mode corresponding to the formation of symmetrical or
72 asymmetrical folds creating multi-lobes (accordion mode) is generated by local buckling and concerns
73 ductile materials such as aluminium or Kevlar fibres (Fig. 1 (a) and (b)). The additional folds leading to
74 the formation of the accordion mode are created by a succession of local buckling events. During this

75 failure mode, energy is absorbed by the plasticization of the folds. Farley and Jones called this mode
76 "folding mode" or "local buckling mode" [31].
77 The "splaying crushing mode" (name given by Hull [32]) or "lamina bending mode" (name given by Farley
78 and Jones [31]) concerns fragile materials. Splaying corresponds to a division of the walls into two parts
79 (Fig 1 (c)). The splaying mode starts with an interlaminar crack or a delamination, which propagates and
80 separates the structure into two parts. The bending of these two branches causes fibres to break, allowing
81 the initial crack to propagate. In this failure mode, energy is absorbed by friction (delaminated plies, debris
82 trapped inside), by matrix cracking, and by fibre failure. The division of the structure into two branches
83 causes the tube to split, generating the appearance of petals. The fragmentation mode also concerns
84 fragile materials and appears after numerous cracks of the order of magnitude of the thickness of the plies
85 (Fig. 1 (d)). The cracks divide the crushing front into multiple pieces of falling debris, which ruins the
86 structure. Most of the time, for fragile composites, crash failure does not occur in a pure splaying or
87 fragmentation mode but as a mixture of the two. The combination of these two modes (splaying and
88 fragmentation) is called "brittle fracturing mode" by Farley and Jones [31].



89

90 Fig. 1 : « Diamond » failure mode (a) AL6060 tube reproduced from [39]) (b) Kevlar/epoxy tube
91 (reproduced from [40]) Splaying mode (c) CFRP tube (reproduced from [27]) Fragmentation mode (d)
92 GFRP tube (reproduced from [32])

93 Kindervater [33] shows that the specific energy absorbed is dependent on the geometrical shape of the
94 crash-box. Compared to a circular tube, a square tube shows 20% less SEA, and a rectangular tube 50%
95 less. Hull [32] also demonstrated the importance of ply orientation on unidirectional glass or carbon fibre
96 laminate tubes. The SEA varies very strongly depending on the orientation, the position, and the number
97 of plies. The static SEA can vary from 6 to 88 J/g. He also defines a "hoop effect", which describes an
98 improvement in the absorption of energy due to stabilization of the crushing when the fibres oriented at
99 0° are confined between layers oriented at 90° . Similarly, Thornton and Edwards [34], using unidirectional
100 glass fibre tubes, have shown the importance of both the "hoop effect" and the presence of fibres oriented
101 at 0° . If the position of the plies is changed to 0° or 90° , the SEA varies by 50%.

102 The two objectives of the present study are therefore:

- 103 • To evaluate the energy absorption capacity under crash of wood in the form of tubes made from
104 poplar veneers, in static and dynamic crushing, and thus to compare not only the performance
105 levels but also the failure modes. Poplar was chosen from among the many wood species
106 available because of its low cost, its ease of manufacture and its availability in the form of plies.
107 As its mechanical characteristics are among the weakest, the results obtained can be considered
108 to represent the least advantageous possibilities of wood.
- 109 • To understand the mechanisms of damage and energy absorption of these tubes and compare
110 them with the findings of other crash studies on known materials, such as composite or metallic
111 materials.

112

113 2. Materials and Methods

114 2.1. Materials and manufacturing.

115 The tubes were manufactured from I214 poplar veneers supplied by the Garnica company [35]. The
116 thickness of the plies was 1 mm. All the tubes produced had 6 plies, with an internal diameter of 50 mm
117 for a length of 120 mm. The total thickness of the tubes was between 6.25 and 6.90 mm. Depending on

118 the configuration and the constraints of the veneer bending process, the thicknesses varied slightly. The
 119 average relative density of the tubes (veneers and glue) was 544 kg/m³. The glue used to bond the
 120 veneers was Kleiberit PUR 510 Fiberbond, a one-component glue based on polyurethane hardening by
 121 reaction with humidity, having an areal density of 250 g/m². The static and dynamic characterization of
 122 the individual ply was not performed in this study and is out-of-the scope of the objective of this paper.
 123 Unlike classical composite materials, the need for characterization in the industry is poor at this level and until
 124 the research is also not so developed. Nevertheless, only static bending tests are available in the literature
 125 [36, 37] and are summarized in the in Table 1:

		Bending		Ref
		Modulus (MPa)	Strength (MPa)	
One-ply (4.3 mm)	Hybrid poplar clone 15 303	5 862	50	(Fang et al. 2012)
Plywood (12 mm)	Poplar clone "I-214"	4 153	24.8	(Baldassino, Zanon, et Zanuttini 1998)

126 Table. 1: Some results on poplar material properties [36, 37].

127 Regarding the forming of the tubes, the stacking of layers at 0° was performed dry. For layers at 90°, it
 128 was necessary to immerse the veneers in water before forming them directly on a mould. They were then
 129 dried at 50 °C for 3.5 hours. Once dry, the veneers were bonded and rolled up using heat-shrinkable
 130 bands, which provided pressure during the crosslinking of the glue at 120 °C for 20 min. The relative
 131 humidity of "dry" veneers oriented at 90 ° was between 5.5 and 12.7%, and was between 8.8 and 9.8%
 132 for veneers oriented at 0°. The tubes were finally cut to the desired length. At one end (Fig.2), a 45°
 133 chamfer was milled over the entire thickness of the tube in order to initiate failure and reduce the load
 134 peak [38].

135 Four configurations were used to study the effect of the stacking sequence: [0₆], [90/0₄/90], [90₂/0₂/90₂],
 136 and [0₄/90₂], 0° corresponding to the longitudinal axis of the tube. For each configuration, three tubes
 137 were crushed in order to assess the repeatability of the results.

138



Fig. 2: Pristine sample [0₄/90₂] - #2

139

140

141

142

143

144

145

146

2.2. Static tests

147 The tests were carried out at a speed of 5 mm/min on an MTS system tension machine equipped with a

148 100 kN load cell and a displacement sensor. The tubes were crushed over $\frac{3}{4}$ of their length, i.e. 90 mm,

149 which was long enough for a stable crushing mechanism to be observed when it existed.

150 Generally, during a stable crash, three phases are observed on the force-displacement curve: a pseudo-

151 linear part up to a peak force, which is followed by the first damage and a transition phase and, finally, a

152 plateau phase. In our case, the apparent linearity of the force-displacement curve corresponded rather to

153 a pseudo-linear phase because, in reality, the chamfer of the tube started to be damaged. Several

154 quantities and performance criteria can be extracted from the force-displacement curve obtained during

155 the crash. The peak force is noted F_{max} . When a force plateau exists, the average force in the plateau is

156 called $F_{plateau}$. The CFE (Crush Force Efficiency) can then be defined as the ratio between the average

157 force and the maximum force ($F_{plateau} / F_{max}$). In general, when designing a shock absorber [39], a CFE as

158 close to 1 as possible is sought, to limit the forces in the rest of the structure during a crash.

159 With regard to energies, two quantities were defined. The first was the total energy dissipated in the tube.

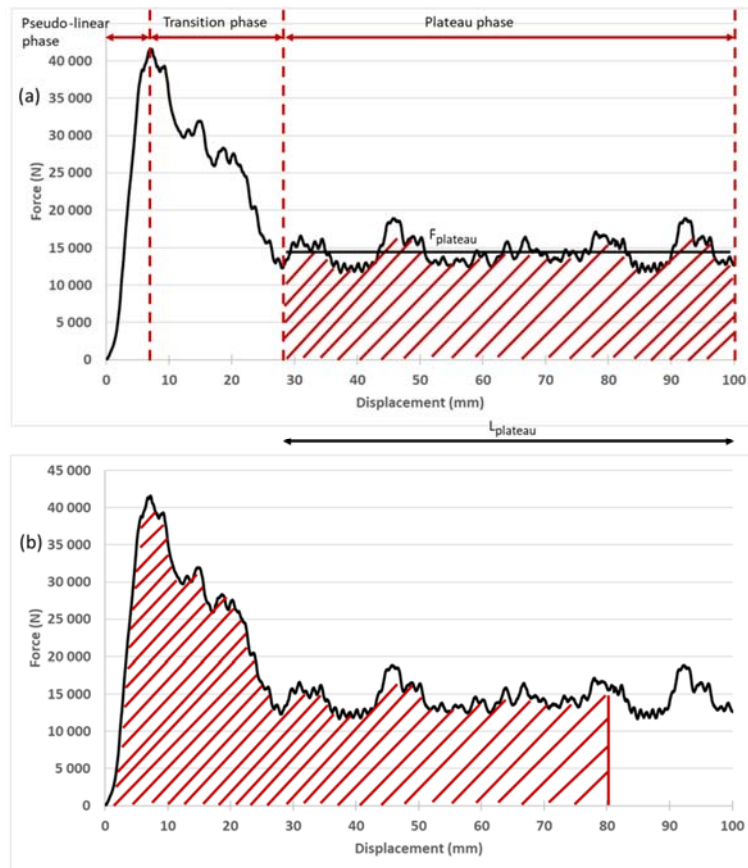
160 It allowed direct comparison of the absorption capacities of various tubes. As the crushed length varied

161 somewhat according to the tests (between 80 and 90 mm), the total energy was calculated only on the
 162 first 80 mm crushed. It is written E_{tot_80mm} here (see Fig. 3 (b)).

163 In this paper, the specific absorption energy was calculated, not from the entire curve, but only from the
 164 stabilized phase of the crushing (Fig. 3 (a)), which therefore corresponded to established absorption mode
 165 and damage mechanisms. Thus, we also defined the energy absorbed in the plateau ($EA_{plateau}$), which
 166 depends on the real length of the stable phase ($L_{plateau}$), and deduced the specific absorption energy

167 during the plateau: $SEA_{plateau} = \frac{F_{plateau}}{\rho \times S}$, in J/g, with ρ the average density of the tube (glue + veneers)

168 and S its cross section.



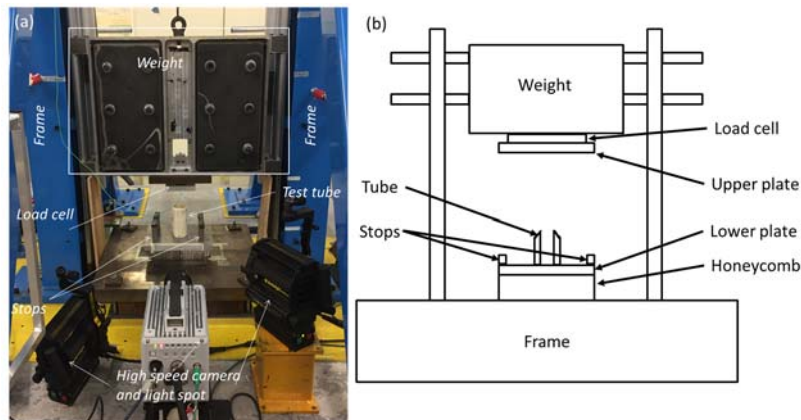
169

170 Fig. 3: Calculation methods for the Energy Absorbed. (a) $EA_{plateau}$ only, (b) EA_{tot_80mm}

171 2.3. Dynamic tests

172 The dynamic tests were carried out using a drop weight tower, at 5.7 m / s (Fig. 4). These tests were
 173 interrupted for post-mortem observations on the samples. They were also filmed using a high-speed
 174 camera during the entire crash.

175 The operating principle of the assembly was as follows: the mass used (180 kg) was calculated so that
176 the kinetic energy available during the impact was significantly greater than the energy necessary to crush
177 85 mm of the tube. We thus obtained a test with an almost constant crushing speed. To stop the crushing
178 after approximately 85 mm, a stop system was used, which allowed the excess energy to be transferred
179 into an absorber (Nomex honeycomb block) located under the sample (Fig. 4).



180

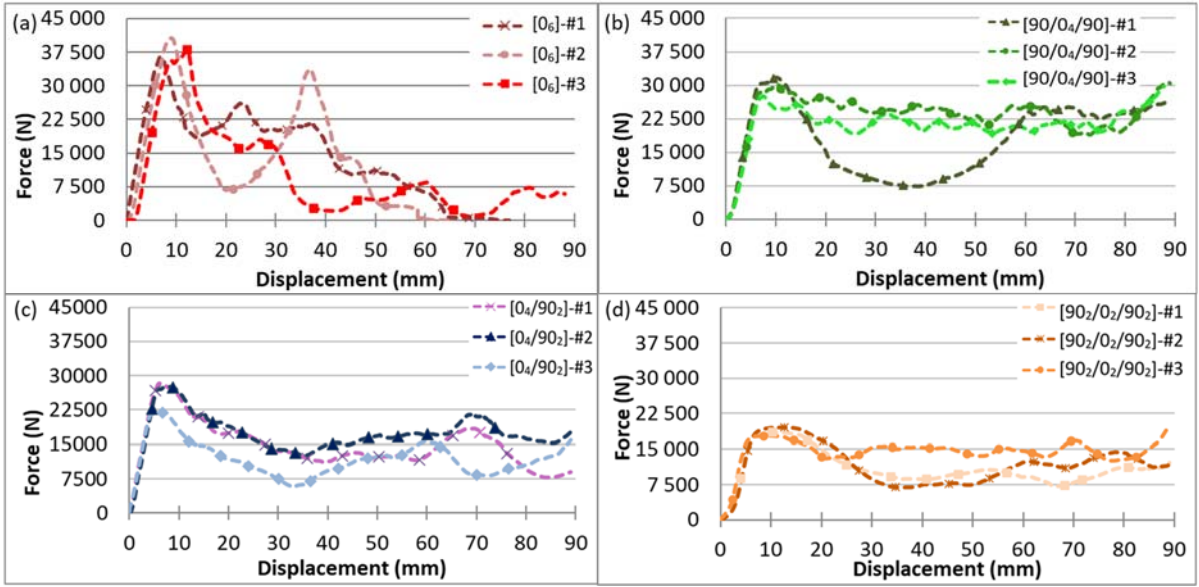
181 Fig. 4: (a) Overview photograph of the dynamic testing setup, (b) Schematic representation

182 A force sensor located between the mass and the upper crushing plate made it possible to obtain the
183 crushing force with an acquisition frequency of 1 MHz. The displacement was calculated by double
184 integration of the force from knowledge of the initial speed given by an optical sensor. No filtering was
185 performed for data extraction. The high speed camera and the force signal were synchronized in order to
186 be able to link the images of the crushing front with the force-displacement curve. **A redundant calculation**
187 **of displacement was also carried out using the camera images for a few samples to verify the accuracy**
188 **of the double integration method.**

189 3. Results and discussion

190 All data are available in Table. 2 and Force-displacement curves for the static response are shown in Fig

191 5.



192

193

Fig. 5: Static force-displacement curves for tubes (a) $[0_6]$ (b) $[90/0_4/90]$ (c) $[0_4/90_2]$ (d) $[90_2/0_2/90_2]$

	g	mm	N	mm	N	$/$	J	J	J/g	
	$Mass$	$Thickness$	F_{max}	$L_{plateau}$	$F_{plateau}$	CFE	$EA_{plateau}$	$EA_{tot,80mm}$	$SEA_{plateau}$	
Static tests	$[0_6]$ - #1	77.4	6.7	36 403	/	/	/	/	/	
	$[0_6]$ - #2	76.0	6.8	40 667	/	/	/	/	/	
	$[0_6]$ - #3	75.3	6.6	38 067	/	/	/	/	/	
	Average	76.2	6.7	38 379	/	/	/	/	/	
	Standard deviation	1.07	0.09	2 149	/	/	/	/	/	
	$[90/0_4/90]$ - #1	76.9	6.9	31 722	74.9	17 039	0.54	1 276	1 368	25.4
	$[90/0_4/90]$ - #2	77.8	6.9	30 220	77.6	24 092	0.80	1 869	1 858	35.5
	$[90/0_4/90]$ - #3	74.9	6.7	27 569	78.1	21 926	0.80	1 712	1 670	33.8
	Average	76.6	6.8	29 837	76.9	21 019	0.71	1 619	1 632	31.6
	Standard deviation	1.8	0.10	2 103	1.7	3 613	0.15	307	247	5.4
$[90_2/0_2/90_2]$ - #1	70.6	6.7	17 798	68.9	14 592	0.82	1 005	1 154	22.2	
$[90_2/0_2/90_2]$ - #2	73.1	6.6	19 541	64.2	10 312	0.53	662	923	16.3	
$[90_2/0_2/90_2]$ - #3	75.7	6.8	18 514	53.7	9 542	0.52	512	866	15.6	
Average	73.1	6.7	19 403	62.2	11 482	0.62	726	981	18.0	
Standard deviation	2.55	0.11	876	7.18	2 721	0.17	253	152	3.6	
$[0_4/90_2]$ - #1	73.5	6.5	28 311	55.3	12 680	0.45	701	1 241	19.9	
$[0_4/90_2]$ - #2	73.3	6.5	27 581	53.9	16 779	0.61	905	1 400	26.4	
$[0_4/90_2]$ - #3	72.4	6.6	22 039	56.7	10 991	0.50	624	939	17.5	
Average	73.0	6.6	25 977	55.3	13 483	0.52	743	1 193	21.3	
Standard deviation	0.59	0.01	3 430	1.4	2 976	0.08	145	234	4.6	
Dynamic tests	$[90/0_4/90]$ - #1	72.0	6.5	41 601	51.5	14 454	0.35	744	1 462	23.2
	$[90/0_4/90]$ - #2	72.5	6.3	45 213	54.9	14 515	0.32	797	1 428	23.1
	$[90/0_4/90]$ - #3	71.0	6.3	44 762	54.0	18 997	0.42	1 025	1 705	31.0
	$[90/0_4/90]$ - #4	72.7	6.3	44 947	55.9	21 143	0.47	1 183	1 759	33.7
	$[90/0_4/90]$ - #5	75.4	6.4	46 717	55.8	22 716	0.49	1 267	1 842	34.9
	$[90/0_4/90]$ - #6	73.2	6.7	47 267	55.2	15 811	0.34	873	1 512	24.9
	Average	73.7	6.5	45 084	54.6	17 939	0.40	982	1 618	28.5
Standard deviation	1.44	0.16	1 951	0.4	3 538	0.07	212	173	5.4	

194

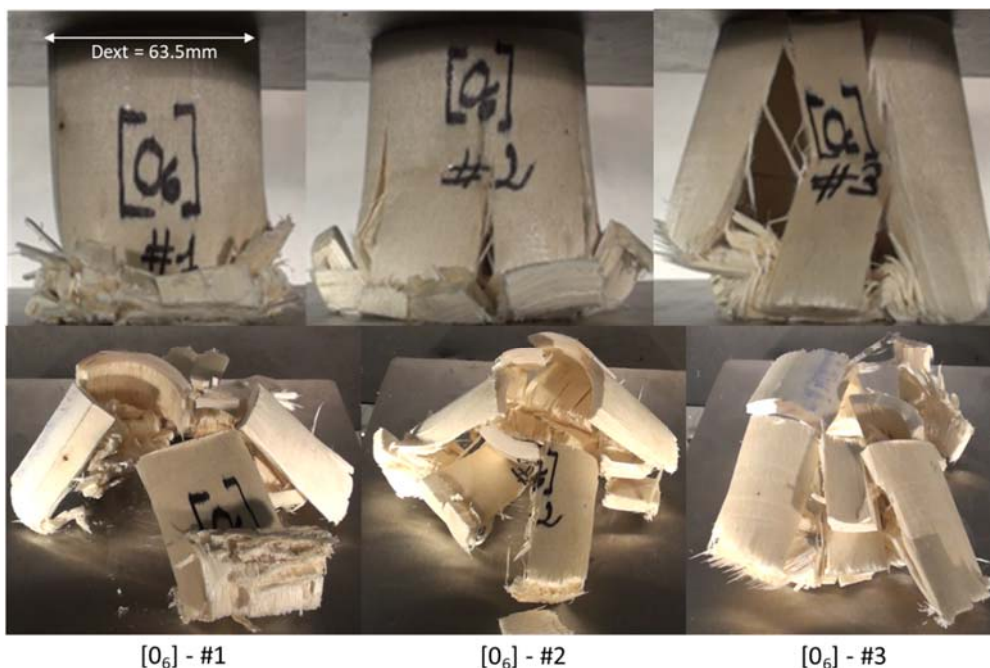
Table. 2: Static and Dynamic test results.

195

196 3.1. Static crushing

197 3.1.1. Results for $[0_6]$ Tubes.

198 The first damage corresponded to the appearance of longitudinal cracking along the fibres after the peak
199 load (Fig. 5 (a)). These cracks cut the tube into several sections (Fig. 6). Then each section began to
200 bend until it broke. The longitudinal crack spread over a large part of the tube, leading to a total loss of
201 stiffness of the tube and marking a crushing force close to 0. For these types of tubes, the absence of a
202 plateau is to be noted and, therefore, energy absorption performance is difficult to exploit and the
203 expression does not necessarily have a clear meaning (Fig. 5 (a)). Delamination between layers also
204 occurred, and fragmentation could also be observed following these failures in fibres at 0° stressed under
205 bending (Fig. 6). It generated the formation of bundles, five large ones (almost half the length of the tube)
206 being counted for tubes # 1 and # 3, and 6 for tube # 2. This failure mode was observed on the three
207 tubes and was repeated although certain cracks did not start to form at the same time, which explains the
208 shift in the force-displacement curves (Fig. 5 (a)). However, this is a very unstable mode of failure and
209 results in oscillations generating a small amount of absorbed energy due to the force falling to 0 N. For
210 this configuration, the energy absorption is not optimal.



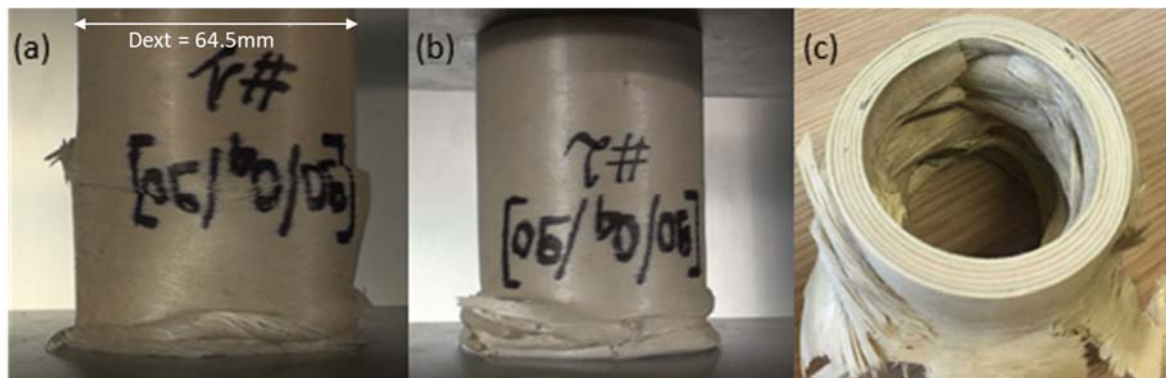
211

212 Fig. 6: Failure patterns of $[0_6]$ tubes under a crush displacement of 40 mm and post-mortem patterns.

213
214

3.1.2. Results for [90/0₄/90] Tubes.

215 The advantage of this configuration was that it permitted observation of the influence of the orientation of
216 the outer and inner layers at 90°, which creates a confinement of the inner layers at 0°. For the first tube
217 (# 1) failure initiation occurred in its middle (Fig. 7 (a)). For the other two other tubes (# 2 and # 3), folds
218 occurred in an asymmetric manner. Once the first fold was created, the tube returned to its initial
219 configuration and could sustain crushing on a portion of the tube that had not yet been damaged. The first
220 fold appeared as soon as the chamfer was crushed. During the crushing and because of the creation of
221 the folds, the fibres at 90° broke and the fibres at 0° bent until they ruptured. The failure modes of the
222 three tubes was quite similar: even though the damage of tube # 1 began halfway up the tube, the same
223 mode of failure occurred during the crushing, which explains the same level of force obtained at the end
224 of the compression. However, the number of folds was not identical in the three tubes.



225

226 Fig. 7: (a) Failure mode of tube [90/0₄/90] - #1 after 20 mm of crushing; (b) tube [90/0₄/90] - #2 after 32 mm
227 of crushing and fold creation; (c) tube [90/0₄/90] - #3 post-mortem pattern

228 The resulting failure mode can be compared to the diamond failure mode [40-42] in tubes made of metallic
229 material, for example aluminium (Fig. 1 (a)), or Kevlar-epoxy composites (Fig. 1 (b)).

230 The force-displacement curve (Fig. 5 (b)) exhibits a load peak followed by the first damage. In
231 configuration [90/0₄/90], unlike configuration [0₆], a plateau occurs after the load peak, except for tube #1.
232 For this tube, as already mentioned, the initiation of failure occurred in the middle. So, the first fold did not
233 form from the start of the crushing and was observed later, with a drop in force at the level of the plateau

234 between about 20 and 50 mm. Then, an increase in the force was observed up to the plateau level for
235 tubes # 2 and # 3. For wood, introducing fibres at 90° helped to stabilize the crushing by confining the
236 fibres at 0°. The stabilization of the crushing linked to the layers at 90° thus prevented transverse
237 longitudinal cracks, made it possible to obtain a plateau on the force-displacement curve (non-existent for
238 the tubes [0₆]) and significantly increased the energy absorbed (1 619 J) and the SEA (31.6 J / g). These
239 tests also showed a relatively low initial peak force compared to the plateau value, resulting in a relatively
240 high CFE (0.71)

241 3.1.3. Results for [90₂/0₂/90₂] Tubes.

242 This configuration showed the influence of the number of layers at 90° on energy absorption. The initiation
243 of damage on tubes # 1 and # 3 was unstable. In fact, it was probably due to an interaction between local
244 buckling at the centre of tubes and overall buckling (Fig. 8). The ruin of tube # 1 spread with
245 interpenetration while the ruin of tube # 3 spread on the opposite side of the chamfer. The damage
246 initiation in tube # 2 occurred as expected on the chamfered side. Thereafter the failure mode of these
247 tubes was similar to that of tubes [90/0₄/90] with formation of folds (Fig. 8). Nevertheless, the folding
248 propagation was stable with regard to the force-displacement curve of each of the tubes (Fig. 5 (d)).
249 However, there were about half as many folds on the configuration [90/0₄/90] (discussed in section 3.1.5),
250 which explains the smaller number of oscillations on the force displacement curve. As with composite
251 laminates, the number of 0° plies was important. Therefore, the energy absorbed and the SEA of these
252 tubes (1 619 J and 31.6 J/g) decreased with respect to the configuration [90/0₄/90] (726 J and 18 J /g).
253 The CFE also decreased slightly from 0.71 to 0.62.

254



255

256 Fig. 8: First line: failure initiation of tubes $[90_2/0_2/90_2]$ after 23.8 mm of crushing; second line: failure

257 patterns after 60 mm of crushing and, last line: post-mortem views.

258 3.1.4. Results for $[0_4/90_2]$ tubes.

259 The objective for this last configuration was to observe the influence of the position of the layers at 90° .

260 Fold formation was again present for the mode of ruin of these tubes. At the beginning of the crushing, it

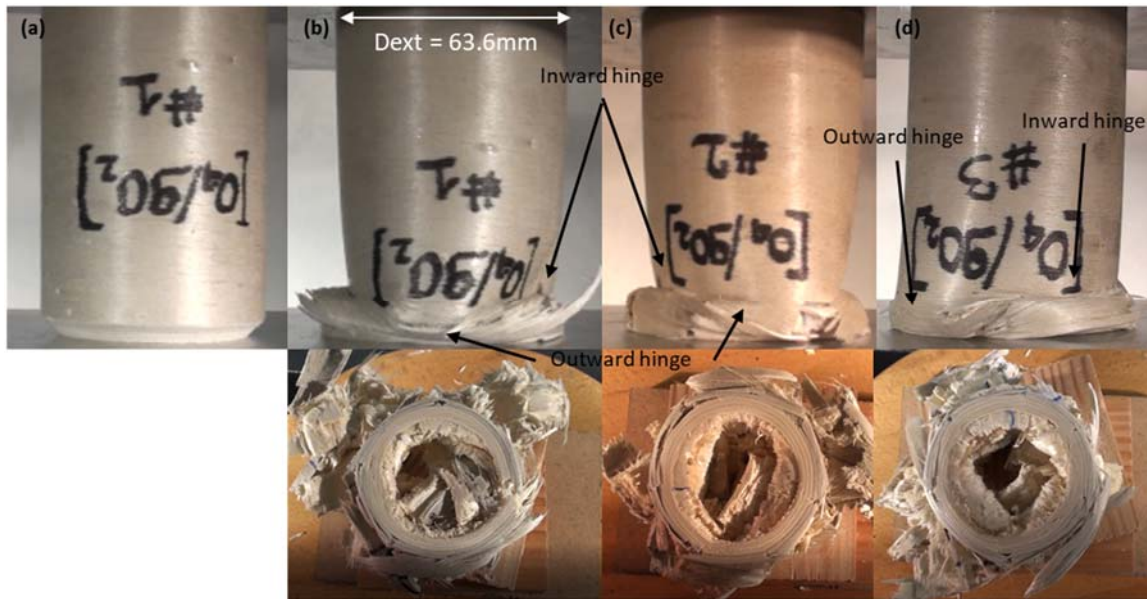
261 was found that the tubes lost their cylindrical geometry, which became oval, corresponding to the

262 formation of a fold in diamond mode, probably because of the unsymmetrical stacking, which created

263 local membrane/bending coupling. At a given height of the tube and on the same plane, two inside folds

264 were created facing each other while, perpendicularly, there were also two folds facing each other, but

265 outwards (Fig. 9). So, on this same plane, 4 folds were visible.



266

267 Fig. 9: Initiation of failure mode of $[0_4/90_2]$ tubes. (a) #1 pristine, (b) #1, (c) #2 (d) #3 between 26 and 27mm
 268 of crushing.

269 The diamond shape appeared at the start of crushing and corresponded to the formation of the plateau
 270 on the force-displacement curve (around 30 mm of crushing) (Fig. 5 (c)). Furthermore, the number of folds
 271 for this configuration was almost twice that with the $[90/0_4/90]$ configuration and, again, can explain why
 272 the oscillations on the force-displacement curve were less marked. The influence of the position of the
 273 layer at 90° is not negligible and has its importance for the amount of energy absorbed. From the
 274 configuration $[90/0_4/90]$ to configuration $[0_4/90_2]$, an average loss of 87.6 J for EA and 10.3 J/g for SEA
 275 should be noted. The CFE dropped by 0.19. Having a 90° fold inside and outside clearly stabilized the
 276 fibres at 0° and induced better confinement than in the case where folds were located outside only.

277 3.1.5. Discussion on the crushing patterns (static).

278 Having no layers oriented at 90° , the tubes $[0_6]$ crushed in a very unstable way. The initiation was marked
 279 by the appearance of bundles characterizing cracking between the fibres in the longitudinal direction. The
 280 propagation of splitting in the direction of the tube led to a significant loss of stiffness of the tube, cutting
 281 the tubes into bundles (Fig. 6). As the tubes no longer satisfied the structural criterion, the initial crushing
 282 length of 90 mm was not respected; the test was interrupted on tubes # 1 and # 2 (zero compression
 283 force). With a layer oriented at 90° , crushing was stabilized, and a gain in absorbed energy was observed.

284 Nevertheless, it is difficult to analyse the situation by looking only at the outer pattern of the tubes from a
285 macroscopic point of view. Therefore, some tubes were cut lengthwise into two half-tubes to gain access
286 to more information about their failure modes (Fig. 10 (a)).

287 Some differences between the two configurations [90/0₄/90] and [90₂/0₂/90₂] were still present. The
288 number of folds was higher for the [90/0₄/90] tubes (Fig. 10 (a)). Other authors [43] have found that
289 inserting foam on thin-walled tubes reduces the buckling length of the folds, thereby increasing their
290 number, and also increases the crushing force. In our case, we can assume that the presence of more
291 fibres at 0° required a greater crushing force, which generated an increase in the number of folds and
292 therefore more energy absorbed.

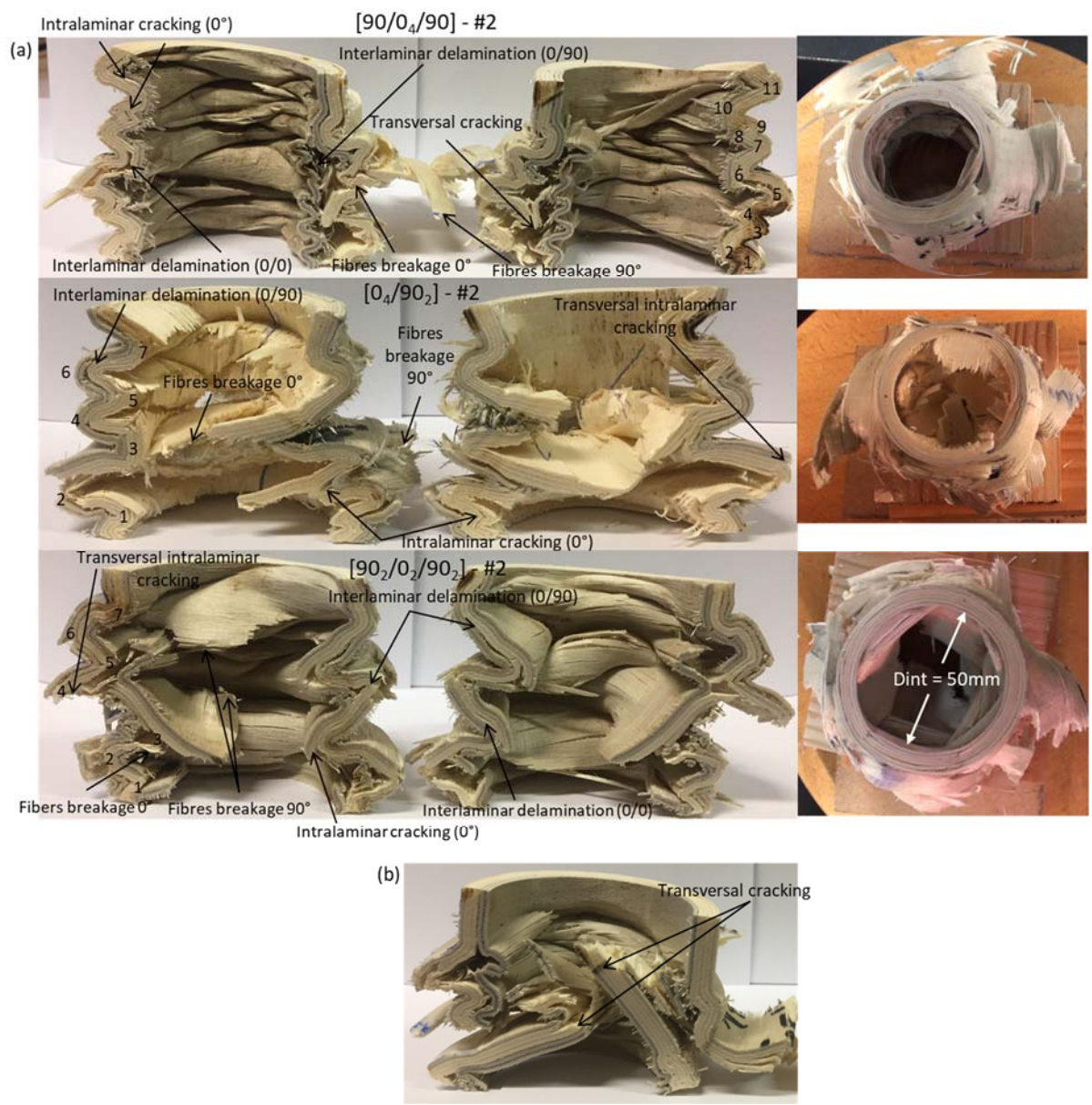
293 For [90/0₄/90] tubes, transversal cracking (i.e. in the thickness of the tube) was visible in the wall of the
294 tube # 1 (Fig.10 (b)). This crack may explain the drop in the crushing force in the plate after the peak load.

295 Such cracks were also found in the other two configurations [0₄/90₂] and [90₂/0₂/90₂]. For tubes [90/0₄/90]
296 # 2 and # 3 and [90₂/0₂/90₂] - # 3, the fibre breakages observed in layers oriented at 90° allowed the
297 appearance of a vertical crack creating petals, although the global failure mode was by local buckling (Fig.
298 10 (a)). In Fig. 10, some 0° layers can be seen to be broken, probably because of the high bending
299 stresses due to the local hinges. However, most of the time, the wooden layers support large local
300 deformations. Delaminations are also observed everywhere, mostly at the 0°/90° interface but it is hard
301 to explain their onset in the failure scenario (before or after the peak load) in this post-mortem analysis.

302 Finally, an elastic return was observed in the length of the tubes. Since the tubes were not 100%
303 damaged, some structural integrity of the tubes remained. Therefore, the tubes unfolded after the release
304 of the compression force. The elastic return is not negligible: the remaining length of the crushed tubes
305 should have been 30 mm, whereas a residual length of around 60 mm was measured.

306 Finally, the overall failure patterns of each configuration having two of the layers oriented at 90° are very
307 similar to each other (local buckling formation, delamination 0/90, etc.) but there are many discrepancies,
308 which can be attributed to several parameters:

- 309 • The fact that the tubes were manufactured manually may have introduced sources of variability:
- 310 the process could have led to a deviation of the angles of the fibres (0° or 90°), due to either the
- 311 cutting or the winding of the veneers, and the bonding could exhibit some defects.
- 312 • In addition to being anisotropic, wood is a very heterogeneous material. It therefore shows
- 313 considerable variability in its properties: humidity, density, spring / winter wood, etc.

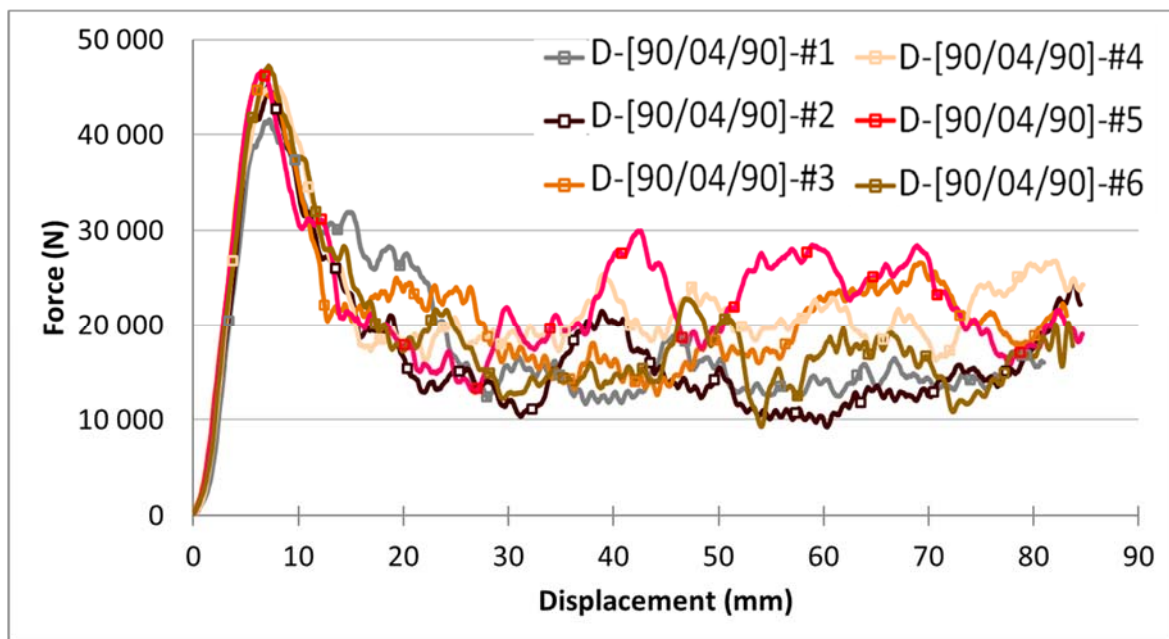


314
 315 Fig. 10: (a) Static crushing modes – the left and right pictures are from the same sample. The figures on
 316 the pictures are used to count the number of folds. (b) Delamination, photo of half-tube $[90/0_4/90] \#1$

317
 318
 319

320 3.2. Dynamic crushing

321 The configuration of the tubes having the best characteristics in terms of energy absorption (EA, SEA and
322 CFE) in static tests was kept for the dynamic tests. Six tubes [90/0₄/90] were crushed in order to see the
323 difference in behaviour and energy absorption in static and dynamic situations. Results are given in Tab.
324 1 and the six dynamic crushing force-displacement curves of the tubes [90/0₄/90] are shown in Fig.11.
325 The general shape of the force-displacement curves is identical to the static case, with the same three
326 phases of initiation, transition and plateau. In terms of performance, two groups of tubes can be identified:
327 tubes 1, 2 and 6 have a SEA between 23.1 and 24.9 J / g while tubes 3, 4 and 5 have a SEA of 31 to 34.9
328 J / g. From the manufacturing point of view, no significant defects that could explain this performance gap
329 were observed from one tube to another. Therefore, this difference can be attributed, as in static crushing,
330 to the variability of the material.

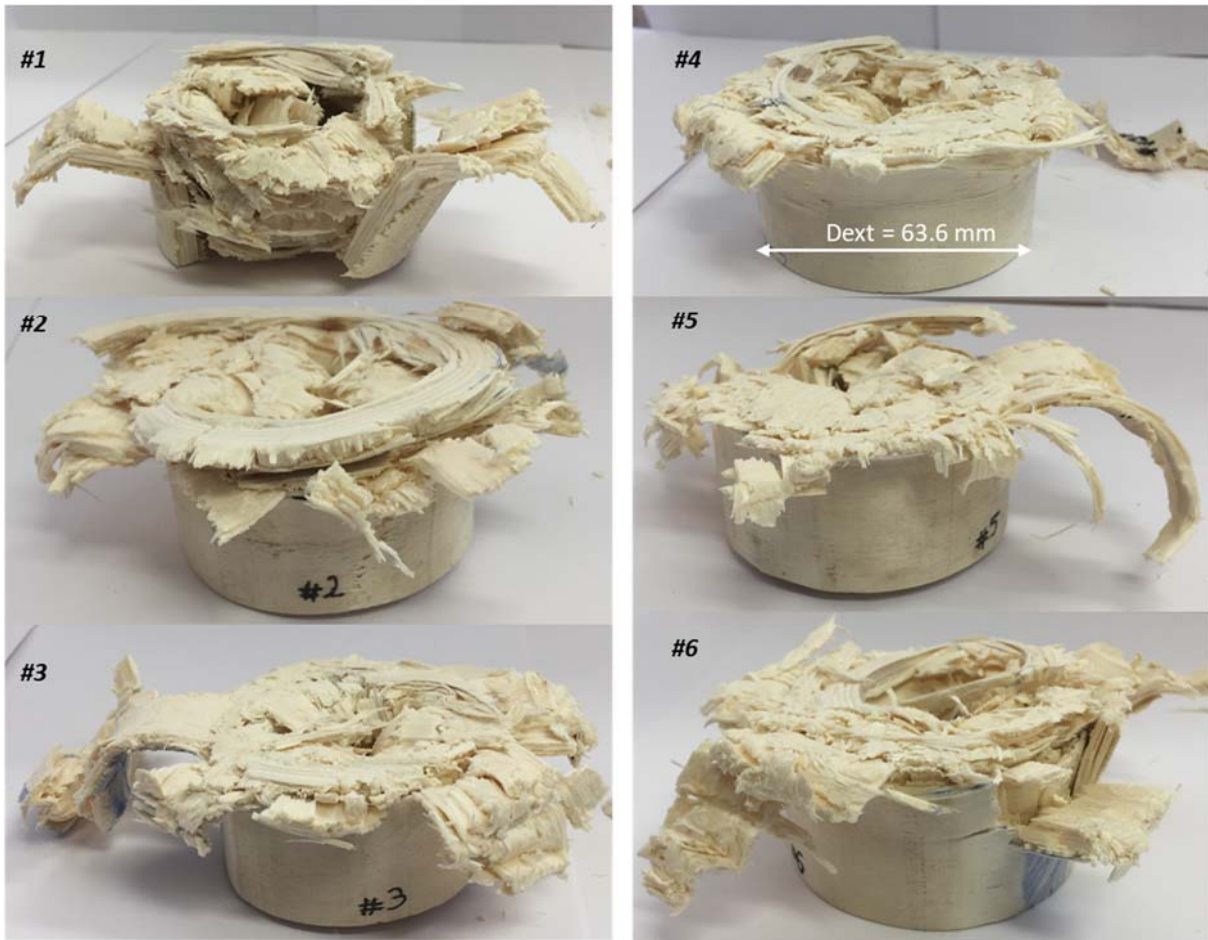


331

332

Fig. 11: Dynamic force-displacement curves for tubes [90/0₄/90]

333 The dynamic failure pattern is almost the same on the six specimens (Fig. 12).



334

335

Fig. 12: Dynamic crushing modes of all 6 tubes [90/0₄/90]

336 Crushing is initiated by the formation of a local fold on the side of the chamfer, recalling the mode of ruin

337 of the tubes in static tests. The formation of the folds generates delaminations, intralaminar cracking and

338 probably wood fibre failures, which divide the tubes into bundles (Fig. 13).

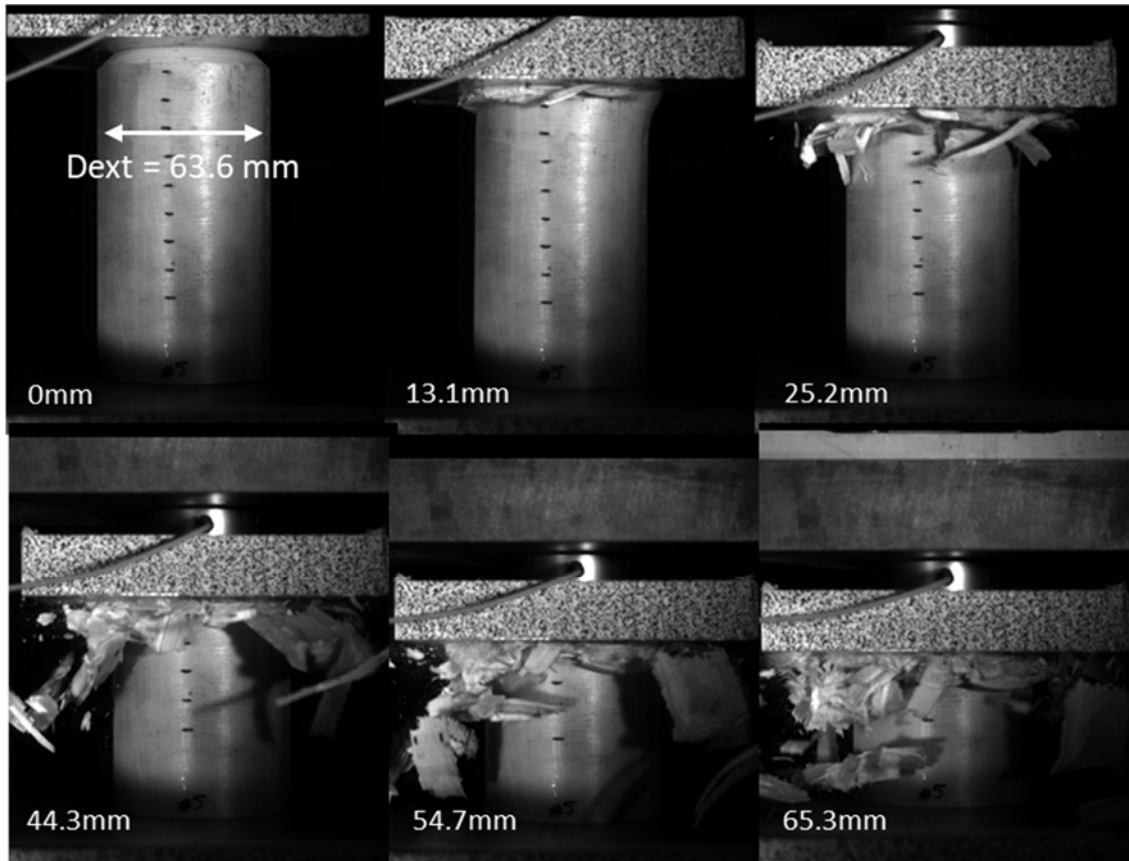


Fig. 13: Failure scenario of tube #5

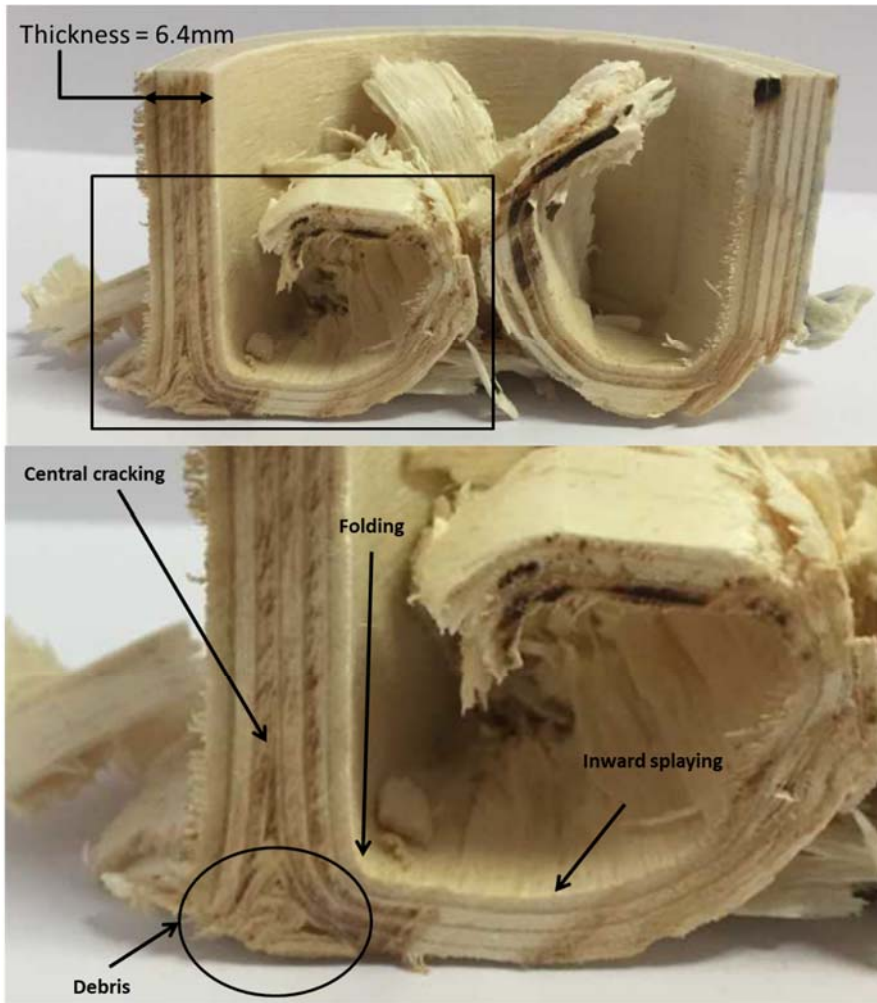
339

340

341 The failures then propagate due to local bending until local fragmentation forms macroscopic debris (Fig.
 342 13). Small debris (almost dust) was also observed. The separation of the tube into a bundle and the
 343 bending of the latter is analogous to splaying. The observation of macroscopic debris allowed us to note
 344 that splaying did not occur in an identical way for all the tubes. By cutting the tubes it was possible to
 345 provide a more precise explanation of the ruin of the tubes used in dynamic tests (Fig. 14). The presence
 346 of debris during the crushing is responsible for the splaying as the debris forces the upper intact part to
 347 separate and splay. When crushing different configurations of carbon-epoxy fibre plates, Guillon [23] also
 348 found an accumulation of debris causing a damaged flare. Depending on the position, the debris will
 349 condition the number of folds that splay inward or outward (Fig. 15).

350 The formation of bundles and their bending allow the creation of petals. The formation of petals has been
 351 observed on crushed CFRP tubes for a long time [27] (Fig. 15). Splaying is also initiated by an interlaminar
 352 crack that dissociates the tubes into bundles. Again, these bundles bend and then form the petals. The

353 geometric shape of the petals (length, width, thickness) are influenced by many parameters such as
354 stiffness, ultimate stresses, tube diameter, and wall thickness.



355

356

Fig. 14: Tube #5 cross section



357

358

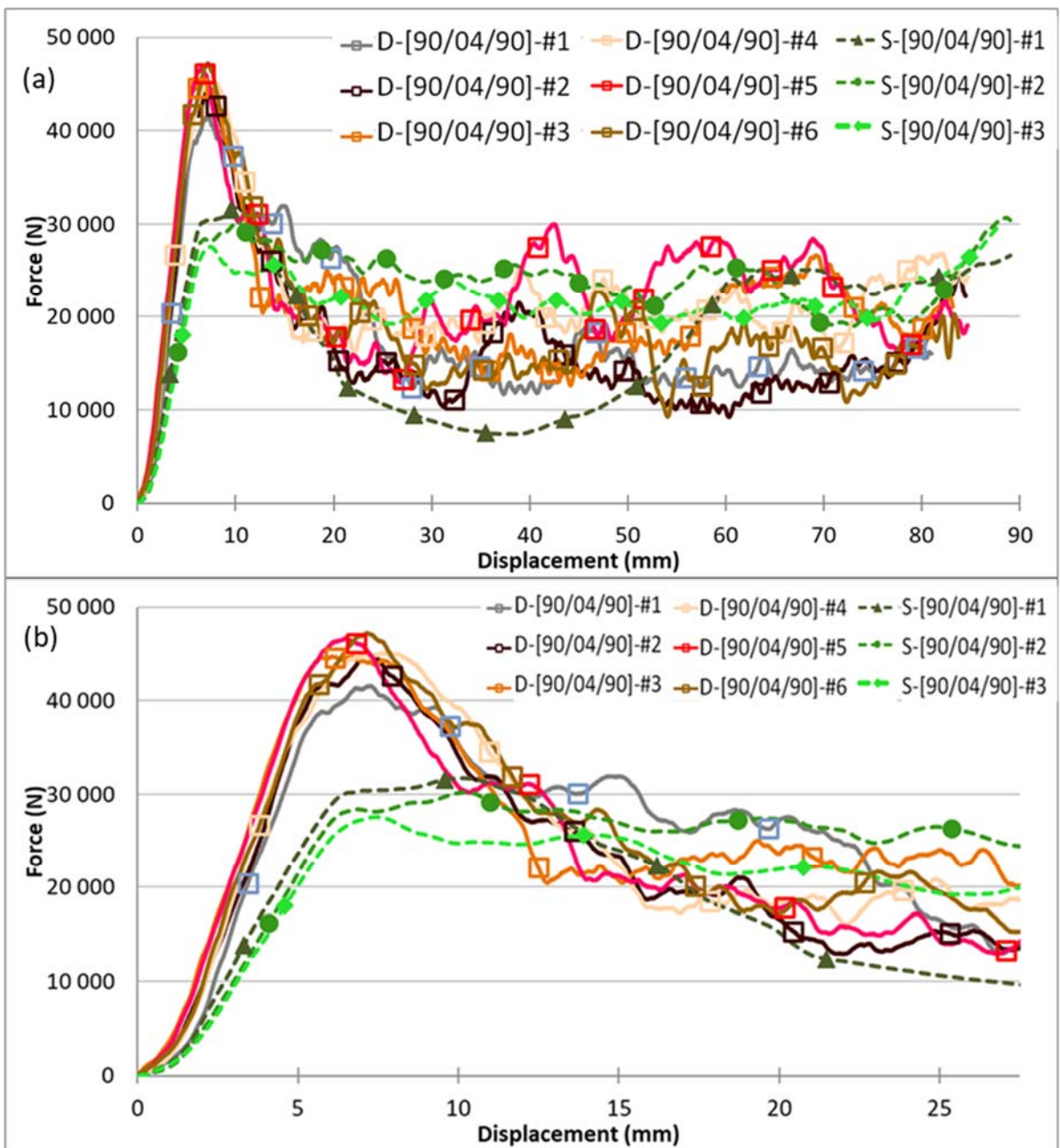
Fig. 15: Petal failure mode for poplar wood.

359

360

361 3.3. Comparison of static and dynamic crushing

362 All the test curves for the [90/0₄/90] specimens are merged in Fig. 16.



363

364 Fig. 16: (a) Comparison of static and dynamic crush curves (S-for static and D- for dynamic) (b) Zoom on
 365 the transition region

366 The first major difference between the static and dynamic curves is the value of the peak load: it is much
 367 higher in dynamic (45,084 N) than in static tests (29,837 N). The second difference is the apparent
 368 stiffness of the tube during pseudo-linear loading. The dynamic stiffness (pseudo-linear slope) is 88%
 369 higher than the static stiffness (515 MPa and 970 MPa for static and dynamic, average values). These

370 two differences have also been found in drop weight tests on poplar [13] and in Hopkinson tests on beech
371 and spruce [10,11]. The transition phase between the peak load and the plateau is also more marked in
372 dynamic than in static crushing. In static situations, as soon as the peak load passes, the plateau is
373 present. Although the plateau can be decreasing, it is obtained between 5 and 10 mm in static (Fig. 16
374 (b)). The peak load is obtained at substantially the same displacement as in static tests, except that the
375 dynamic transition phase ends at around 15 mm (12.5 mm for the shortest transition phase, obtained for
376 tube 4). The end of the pseudo-linear phase, corresponding to the moment when the first damage occurs
377 and when there is a fall in force, is around 6-7 mm of displacement for static or dynamic tests. This value
378 corresponds closely to the value of the height of the chamfer, which therefore appears to be responsible
379 for the end of this phase.

380 In addition, the difference between the maximum force and the minimum force observed on the plate is
381 greater in dynamic loading (up to 15,600 N) than in static (11,700 N if the unstable crushing of tube # 1 is
382 omitted). On the other hand, due to the increase in the peak load, the CFE ratio decreases in dynamic
383 loading, from 0.71 to 0.40. Finally, the other performance levels (Tab. 1), whether for the average force
384 (21,019 N in static - 17,939 N in dynamic), the energy absorbed (1,632 J in static - 1,618 J dynamic) or
385 the SEA (31.6 J/g static - 28.5 J/g dynamic), are almost identical between static and dynamic crushing.
386 During Hopkinson or weight-down crushing to assess the effect of the speed of the stress on the behaviour
387 of the wood material [9–13], it was found that the average stress increased with the dynamic effect,
388 causing an increase of the energy absorbed and therefore of the SEA.

389 In this study, the dynamic failure mode differs from the static one. In static, the crushing is stable with
390 creation of folds while the dynamic tubes have a failure initiation identical to the static (formation of a fold)
391 but subsequent propagation is by splaying and fragmentation creating macroscopic and microscopic
392 debris (Fig. 17).



393

394 Fig. 17: Comparison of the failure scenario between a static and a dynamic tests at iso-displacement
 395 [90/0₄/90] - #2 specimen for static - [90/0₄/90] - #1 specimen for dynamic.

396 The change in static-dynamic failure mode can be explained by the viscoelastic nature of wood. Its
 397 constituents (lignin, cellulose, and hemicellulose) have a behaviour that changes with the strain rate. This
 398 can be shown by the increase in the apparent stiffness (mentioned above). Therefore, in static crushing,
 399 the wood has a ductile character, which enables folds to form, while in dynamic, the fragile character
 400 takes over and generates a fragile mode with the creation of multiple macroscopic debris. *In addition, the*
 401 *glue can have an important influence.* It is thus difficult to conclude that (F_{plateau} , $EA_{\text{tot}_80\text{mm}}$, SEA_{plateau})
 402 are almost identical between the static and the dynamic regimes.

403 The transition from static to dynamic crushing is also an issue for composite materials, particularly as far
 404 as the evolution of performances is concerned. Do they increase or decrease in dynamic crushing? The

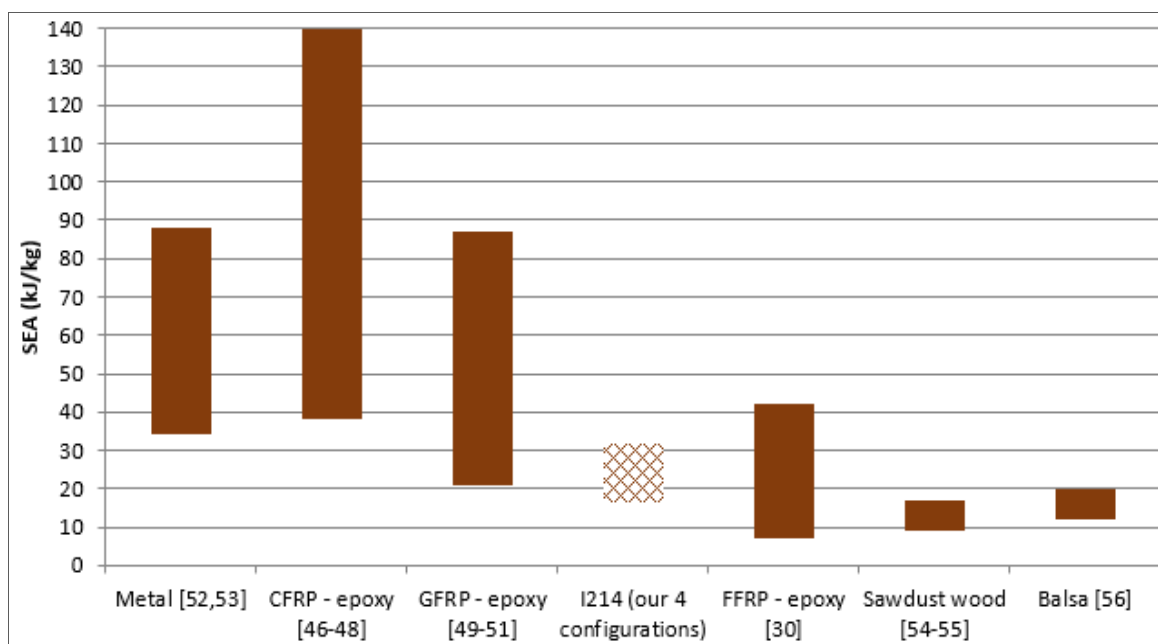
405 works of Farley and Jones [31] attribute the increase in crash characteristics to the dependence of material
406 properties on the strain rate, especially for Kevlar fibres but also for the matrix. In their study, Mamalis et
407 al. [44] obtained different failure modes between static and dynamic loading, thus explaining the variation
408 in performance. McGregor et al. [45] attribute the lower performance in dynamic loading to the fact that
409 there is more transverse shear in the corners of the tubes in dynamic failure, associated with a
410 deterioration of the fibre/matrix interface and a fragile behaviour of the matrix. David et al. [46] observed
411 that the length of the petals was longer in static loading, leading to more cracking, and increased friction
412 in delamination and at the interface of the plates. In dynamic loading, the matrix becomes more fragile,
413 its stiffness increases and its toughness decreases, leading to a reduction in the splaying lengths. Finally,
414 Brighton et al. [47] attribute the decrease in dynamic properties to the radius of curvature of the petals,
415 which is smaller in static and leads to more damage.

416

417 3.4 Summary

418 According to the literature, in terms of SEA, wood shows poorer performance than composite or metallic
419 materials but remains interesting thanks to its carbon footprint, its recyclability, and its material cost, which
420 is very low compared to those of composite materials (the cost of poplar veneer l214 in 1240x2200 mm²
421 format is about € 2.5/veneer while that of CFRP is € 34/m² on average). The SEA of tubes made of carbon
422 fibre composite materials with an epoxy resin ranges from 38 J/g [48], with an internal diameter of 50 mm
423 and a $\pm 45^\circ$ and 0° stacking sequence, to 140 J/g, with the same internal diameter but a [(0/90)/(0)₈/(0/90)]
424 sequence [49] (Fig. 18) and can reach 227 J/g in presence of PEEK resin with a tube 55 mm in diameter
425 and 2.66 mm thick [50]. Glass fibres have a slightly lower potential, from 21 J/g [51] and 87 J/g [52] for
426 semi-hexagonal profiles with unidirectional plies oriented at 0° and 90° to a 39.3 mm diameter tube of 3
427 mm thickness, to a maximum of 195 J/g for a PEEK resin [53] obtained on a 55 mm diameter tube with a
428 thickness of 2.65 mm and fibre orientation of $\pm 10^\circ$. If we consider metallic materials, the SEA can vary
429 from 34 to 88 J/g [54,55], the maximum SEA being obtained with Al 6061 on a 38.1 mm diameter tube

430 with 2.4 mm thickness. Flax tubes ranging from 36 mm to 82 mm in diameter have shown an interesting
 431 potential varying from 7 to 42 J/g [30]. Researchers have also tried to recycle wood chips by integrating
 432 them as core material in PVC (external diameter of 84 mm with 2.3 mm wall thickness) and aluminium
 433 (38 mm inner diameter and 1.2 mm wall thickness) tubes, and have obtained SEA values between 9 and
 434 17 J/g [56, 57]. Finally, with 100 x 100 x 15.5 mm³ plates, as a core material associated with glass fibre
 435 skins, solid balsa has shown a SEA of between 12 and 20 J/g depending on the triggers used [58].



436
437
438 Fig. 18: SEA of various materials

439 4. Conclusions and perspectives

440 Static and dynamic crushing performances are quite promising for a natural and environmentally friendly
 441 material like wood. The tests have shown that:

- 442 • Orienting all the poplar layers at 0° is not a good choice as it generates an unstable failure mode
443 with very low energy absorption.
- 444 • As soon as a 90° layer is present outside and inside (or only outside), this produces a "hoop"
445 effect and the tube will have a stable crushing mode with a plateau whatever the configuration.

- 446 • Too many layers at 90° are not necessarily effective in terms of the amount of energy absorbed:
447 loss of 43% of SEA between the configurations [90₂/0₂/90₂] and [90/0₄/90].
- 448 • The position of the layers at 90° also has an influence on the amount of energy absorbed. In fact,
449 in the configurations [0₄/90₂] and [90/0₄/90], a gain of 33% of SEA is obtained by completely
450 confining the layers at 0°. The "hoop" effect found for composite materials is also found here.
- 451 • In terms of static failure modes, the presence of 90° plies allows successive and asymmetrical
452 formation of folds generated by local buckling. In dynamic tests, the failure mode changes, with
453 the apparition of splaying and fragmentation generating macroscopic and microscopic debris.
- 454 • The best of the static configurations studied, and used in dynamic tests, was [90/0₄/90], which
455 reached an average absorbed energy of 1 632 J in static and 1 618 J in dynamic configurations,
456 with an average SEA of 30 J/g.
- 457 • In dynamic testing, the peak load and the stiffness are significantly increased and the SEA is
458 almost identical. The CFE is also significantly lower in dynamic. Finally, the transition phase is
459 more significant in dynamic than in static loading.

460 These results are very promising for the future of the use of wood-based eco-materials for crash
461 applications. Although the levels of SEA reached are a quarter of those obtained on the best composite
462 materials, the composite materials are 40 times as expensive as the wood-based ones. In addition, the
463 poplar selected for this study is one of the least mechanically efficient woods and it is likely that better
464 quality woods would have higher SEA. In addition, to better understand the crush behaviour of wood
465 tubes, advanced modelling is necessary. A very limited number of papers have dealt with the subject [17]
466 so far and a research effort has to be made to develop material damage models for wood plies, together
467 with efficient modelling strategies.

468

469 5. Acknowledgements

470 The authors thank the French Government for providing financial support and the Garnica company for
471 providing l214 veneers for this study.

472 6. References

473 [1] Laboratory FP. Wood Handbook Wood as an Engineering Material. United States Department of
474 Agriculture Forest Service; 2010.

475

476 [2] Bergman R, Puettmann M, Taylor A, Skog KE. The Carbon Impacts of Wood Products. Forest Products
477 Journal: 2014;64:220-231. <https://doi.org/10.13073/FPJ-D-14-00047>

478

479 [3] Bucci V, Corigliano P, Crupi V, Epasto G, Guglielmino E, Marinò A. Experimental investigation on Iroko
480 wood used in shipbuilding. Proceedings of the Institution of Mechanical Engineers, Part C: Journal of
481 Mechanical Engineering Science 2017;231:128–39. <https://doi.org/10.1177/0954406216674495>.

482

483 [4] Zenkerts D. The handbook of sandwich construction. Engineering Materials Advisory Services Ltd.
484 United Kingdom: 1997.

485

486 [5] Susainathan J, Eyma F, De Luycker E, Cantarel A, Castanie B. Manufacturing and quasi-static bending
487 behavior of wood-based sandwich structures. Composite Structures 2017;182:487–504.
488 <https://doi.org/10.1016/j.compstruct.2017.09.034>

489

490 [6] Butler N. Computer modelling of wood-filled impact limiters. Nuclear Engineering and Design
491 1994;150:417–424; [https://doi.org/10.1016/0029-5493\(94\)90161-9](https://doi.org/10.1016/0029-5493(94)90161-9)

492

493 [7] CANPLY. Eléments de calcul du contreplaqué 1997.

494

495 [8] Johnson W. Historical and Present-Day References Concerning Impact on Wood. International Journal
496 on impact Engineering 1986; 4:161-174. [https://doi.org/10.1016/0734-743X\(86\)90003-5](https://doi.org/10.1016/0734-743X(86)90003-5).

497

498 [9] Reid S.R., Peng C. Dynamic uniaxial crushing of wood. International Journal on impact Engineering
499 1997; 19:531-570. [https://doi.org/10.1016/S0734-743X\(97\)00016-X](https://doi.org/10.1016/S0734-743X(97)00016-X)

500

501 [10] Wouts J, Haugou G, Oudjene M, Morvan H, Coutellier D. Strain rate effects on the compressive
502 response of wood and energy absorption capabilities - Part B: Experimental investigation under rigid
503 lateral confinement. Composite Structures 2018. <https://doi.org/10.1016/j.compstruct.2018.07.001>.

504

505 [11] Wouts J, Haugou G, Oudjene M, Coutellier D, Morvan H. Strain rate effects on the compressive
506 response of wood and energy absorption capabilities – Part A: Experimental investigations. Composite
507 Structures 2016;149:315–328. <https://doi.org/10.1016/j.compstruct.2016.03.058>.

508

509 [12] Pang S, Liang Y, Tao W, Liu Y, Huan S, Qin H. Effect of the Strain Rate and Fiber Direction on the
510 Dynamic Mechanical Properties of Beech Wood. Forests 2019, 10(10), 881;
511 <https://doi.org/10.3390/f10100881>

512

513 [13] Adalian C, Morlier P. “WOOD MODEL” for the dynamic behaviour of wood in multiaxial compression.
514 Holz Als Roh- Und Werkstoff 2002;60:433–9. <https://doi.org/10.1007/s00107-002-0333-x>.

515

- 516 [14] Demircioğlu TK, Balıkoğlu F, Inal O, Arslan N, Ataş A. Experimental investigation on low-velocity
517 impact response of woodskinned sandwich composites with different core configurations. *Materials Today*
518 *Communications* 2018;17:31-39. <https://doi.org/10.1016/j.mtcomm.2018.08.003>
519
- 520 [15] Smardzewski J. Wooden sandwich panels with prismatic core – Energy absorbing capabilities;
521 *Composite Structures* 2019;230:111535. <https://doi.org/10.1016/j.compstruct.2019.111535>
522
- 523 [16] Susainathan, J., Eyma, F., De Luycker, E., Cantarel, A., Castanie, B. Experimental investigation of
524 impact behavior of wood-based sandwich structures. *Composites Part A: Applied Science and*
525 *Manufacturing* 2018;109,10-19. <https://doi.org/10.1016/j.compositesa.2018.02.029>
526
- 527 [17] Susainathan, J., Eyma, F., De Luycker, E., Cantarel, A., Castanie, B. Numerical modeling of impact
528 on wood-based sandwich structures. *Mechanics of Advanced Materials and Structures*, on line,
529 <https://doi.org/10.1080/15376494.2018.1519619>
530
- 531 [18] Susainathan J, Eyma F, De Luycker E, Cantarel A, Bouvet C, Castanie B. Experimental investigation
532 of compression and compression after impact of wood-based sandwich structures. *Composite Structures*
533 2019;220:236–49. <https://doi.org/10.1016/j.compstruct.2019.03.095>.
534
- 535 [19] Nguyen XT, Hou S, Liu T, Han X. A potential natural energy absorption material – Coconut mesocarp: Part A:
536 Experimental investigations on mechanical properties. *International journal of mechanical sciences*, 2016, 115-116:
537 564-573. <https://doi.org/10.1016/j.ijmecsci.2016.07.017>
538
- 539 [20] Liu T, Hou S, Nguyen X, Han X. Energy absorption characteristics of sandwich structures with composite
540 sheets and bio coconut core. *Composites Part B: Engineering*, 2017, 114: 328-338.
541 <https://doi.org/10.1016/j.compositesb.2017.01.035>
542
- 543 [21] Lu C, Hou S, Zhang Z, Chen J, Li Q, Han X. The mystery of coconut overturns the crashworthiness design of
544 composite materials *International journal of mechanical sciences*, 2020, 168: 105244.
545 <https://doi.org/10.1016/j.ijmecsci.2019.105244>
546
- 547 [22] Neveu F, Castanié B, Olivier P. The GAP methodology: A new way to design composite structures
548 *Materials & Design* 2019;172:107755. <https://doi.org/10.1016/j.matdes.2019.107755>
549
- 550 [23] Guillon D. Etude des mécanismes d'absorption d'énergie lors de l'écrasement progressif de
551 structures composites à base de fibre de carbone. PhD Thesis. Institut Supérieur de l'Aéronautique et de
552 l'Espace, ISAE, Ecole doctorale : Mécanique, énergétique, génie civil et procédés, 2008.
553
- 554 [24] Kim J-S, Yoon H-J, Shin K-B. A study on crushing behaviors of composite circular tubes with different
555 reinforcing fibers. *International Journal of Impact Engineering* 2011;38:198-207.
556 <https://doi.org/10.1016/j.ijimpeng.2010.11.007>
557
- 558 [25] Ataabadi PB, Karagiozova D, Alves M. Crushing and energy absorption mechanisms of carbon fiber-
559 epoxy tubes under axial impact. *International Journal of Impact Engineering* 2019;131:74-189.
560 <https://doi.org/10.1016/j.ijimpeng.2019.03.006>
561
- 562 [26] Wang Y, Feng J, Wu J, Hu D. Effects of fiber orientation and wall thickness on energy absorption
563 characteristics of carbon-reinforced composite tubes under different loading conditions. *Composite*
564 *Structures* 2016;153:356–368. <https://doi.org/10.1016/j.compstruct.2016.06.033>.
565

566 [27] Hamada H, Coppola JC, Hull D, Maekawa Z, Sato H. Comparison of energy absorption of
567 carbon/epoxy and carbon/PEEK composite tubes. *Composites* 1992;23:245–252.
568 [https://doi.org/10.1016/0010-4361\(92\)90184-v](https://doi.org/10.1016/0010-4361(92)90184-v).
569

570 [28] Song H-W, Du X-W, Zhao G-F. Energy Absorption Behavior of Double-Chamfer Triggered Glass/Epoxy
571 Circular Tubes. *J Compos Mater* 2002;36:2183–98. <https://doi.org/10.1177/0021998302036018515>.
572

573 [29] Hu D, Zhang C, Ma X, Song B. Effect of fiber orientation on energy absorption characteristics of glass
574 cloth/epoxy composite tubes under axial quasi-static and impact crushing condition. *Composites Part A:
575 Applied Science and Manufacturing* 2016;90:489–501.
576 <https://doi.org/10.1016/j.compositesa.2016.08.017>.
577

578 [30] Yan L, Chou N. Crashworthiness characteristics of flax fibre reinforced epoxy tubes for energy
579 absorption application. *Materials & Design* 2013;51:629–640.
580 <https://doi.org/10.1016/j.matdes.2013.04.014>.
581

582 [31] Farley GL, Jones MR. Energy absorption capability of composite tubes and beams. PhD Thesis.
583 NASA TM 10634, 1989.
584

585 [32] Hull D. A unified approach to progressive crushing of fibre-reinforced composite tubes. *Composites
586 Science and Technology* 1991;40:377–421. [https://doi.org/10.1016/0266-3538\(91\)90031-j](https://doi.org/10.1016/0266-3538(91)90031-j).
587

588 [33] Kindervater CM. Energy absorption of composites as an aspect of aircraft structural crash-resistance.
589 *Developments in the Science and Technology of Composite Materials*, Springer Netherlands; 1990, p.
590 643–651. https://doi.org/10.1007/978-94-009-0787-4_89.
591

592 [34] Thornton PH, Edwards PJ. Energy absorption in composite tubes. *Journal of Composite Materials*
593 1982;16:521–545. <https://doi.org/10.1177/002199838201600606>.
594

595 [35] Garnica. <http://www.garnica.one/en>. Accessed 02 April 2020
596

597 [36] Baldassino N, Zanon P, Zanuttini R. Determining mechanical properties and main characteristic
598 values of Poplar plywood by medium-sized test pieces . *Materials and Structures* 1998;31(1): 64-67.
599 <https://doi.org/10.1007/BF02486416>.
600

601 [37] Fang CH, Mariotti N, Cloutier A, Koubaa A, Blanchet P. Densification of Wood Veneers by
602 Compression Combined with Heat and Steam. *European Journal of Wood and Wood Products* 2012; 70
603 (1-3):155-63. <https://doi.org/10.1007/s00107-011-0524-4>.
604

605

606 [38] Siromani D, Henderson G, Mikita D, Mirarchi K, Park R, Smolko J, et al. An experimental study on
607 the effect of failure trigger mechanisms on the energy absorption capability of CFRP tubes under axial
608 compression. *Composites Part A: Applied Science and Manufacturing* 2014;64:25–35.
609 <https://doi.org/10.1016/j.compositesa.2014.04.019>.
610

611 [39] Blazy J-S. Comportement mécanique des mousses d'aluminium : caractérisations expérimentales
612 sous sollicitations complexes et simulations numériques dans le cadre de l'élasto-plasticité compressible.
613 PhD Thesis. Ecole Nationale Supérieure des Mines de Paris, 2003.
614

615 [40] Andrews KRF, England GL, Ghani E. Classification of the axial collapse of cylindrical tubes under
616 quasi-static loading. *International Journal of Mechanical Sciences* 1983;25:687–696.
617 [https://doi.org/10.1016/0020-7403\(83\)90076-0](https://doi.org/10.1016/0020-7403(83)90076-0).
618

619 [41] Al Galib D, Limam A. Experimental and numerical investigation of static and dynamic axial crushing
620 of circular aluminum tubes. *Thin-Walled Structures* 2004;42:1103–37.
621 <https://doi.org/10.1016/j.tws.2004.03.001>.
622

623 [42] Dubey DD, Vizzini AJ. Testing Methods for Energy Absorption of Kevlar/Epoxy. *J Am Helicopter Soc*
624 1999;44:179–87. <https://doi.org/10.4050/JAHS.44.179>.
625

626 [43] Baroutaji A, Sajjia M, Olabi A-G. On the recent crashworthiness performance of thin walled energy
627 absorbers: recent advances and future developments. *Thin-Walled Structures* 118 137-163 2017.
628

629 [44] Mamalis AG, Manolakos DE, Ioannidis MB, Papapostolou DP. On the response of thin-walled CFRP
630 composite tubular components subjected to static and dynamic axial compressive loading: experimental.
631 *Composite Structures* 2005;69:407–420. <https://doi.org/10.1016/j.compstruct.2004.07.021>.
632

633 [45] McGregor C, Vaziri R, Poursartip A, Xiao X. Axial crushing of triaxially braided composite tubes at
634 quasi-static and dynamic rates. *Composite Structures* 2016;157:197–206.
635 <https://doi.org/10.1016/j.compstruct.2016.08.035>.
636

637 [46] David M, Johnson AF, Voggenreiter H. Analysis of Crushing Response of Composite Crashworthy
638 Structures. *Appl Compos Mater* 2013;20:773–87. <https://doi.org/10.1007/s10443-012-9301-8>.
639

640 [47] Brighton A, Forrest M, Starbuck M, Erdman D, Fox B. Strain Rate Effects on the Energy Absorption
641 of Rapidly Manufactured Composite Tubes. *Journal of Composite Materials* 2009;43:2183–200.
642 <https://doi.org/10.1177/0021998309344646>.
643

644 [48] Schultz MR. Energy absorption capacity of graphite-epoxy composite tubes. Master’s Thesis. Virginia
645 Polytechnic Institute and State University, 1998.
646

647 [49] Chambe J, Bouvet C, Dorival O, Ferrero J. Energy absorption capacity of composite thin-wall circular
648 tubes under axial crushing with different trigger initiations. *Journal of Composite Materials*
649 2019;002199831987722. <https://doi.org/10.1177/0021998319877221>.
650

651 [50] Hamada H, Ramakrishna S. Scaling effects in the energy absorption of carbon-fiber/PEEK composite
652 tubes. *Composites Science and Technology* 1995;55:211–21. [https://doi.org/10.1016/0266-3538\(95\)00081-X](https://doi.org/10.1016/0266-3538(95)00081-X).
653
654

655 [51] Esnaola A, Ulacia I, Aretxabaleta L, Aurrekoetxea J, Gallego I. Quasi-static crush energy absorption
656 capability of E-glass/polyester and hybrid E-glass–basalt/polyester composite structures. *Materials &*
657 *Design* 2015;76:18–25. <https://doi.org/10.1016/j.matdes.2015.03.044>.
658

659 [52] Ochelski S, Gotowicki P. Experimental assessment of energy absorption capability of carbon-epoxy
660 and glass-epoxy composites. *Composite Structures* 2009;87:215–24.
661 <https://doi.org/10.1016/j.compstruct.2008.01.010>.
662

- 663 [53] Hamada H, Ramakrishna S. Effect of Fiber Material on the Energy Absorption Behavior of
664 Thermoplastic Composite Tubes. *Journal of Thermoplastic Composite Materials* 1996;9:259–79.
665 <https://doi.org/10.1177/089270579600900304>.
666
- 667 [54] Farley GL. Energy absorption of composite materials. *Journal of Composite Materials* 1983;17:267–
668 279. <https://doi.org/10.1177/002199838301700307>.
669
- 670 [55] Saito H, Chirwa EC, Inai R, Hamada H. Energy absorption of braiding pultrusion process composite
671 rods. *Composite Structures* 2002;55:407–417. [https://doi.org/10.1016/s0263-8223\(01\)00160-x](https://doi.org/10.1016/s0263-8223(01)00160-x).
672
- 673 [56] Singace AA. Collapse behaviour of plastic tubes filled with wood sawdust. *Thin-Walled Structures*
674 2000;37:163–187. [https://doi.org/10.1016/s0263-8231\(00\)00012-4](https://doi.org/10.1016/s0263-8231(00)00012-4).
675
- 676 [57] Kiran R, Khandelwal N, Tripathi P. Collapse behaviour and energy absorption of aluminium tubes
677 filled with wood sawdust. *International Journal of Engineering Research and Reviews* 2014.
678
- 679 [58] Lindstrom A, Hallstrom S. Energy absorption of SMC/balsa sandwich panels with geometrical
680 triggering features. *Composite Structures* 2010;92:2676–2684.
681 <https://doi.org/10.1016/j.compstruct.2010.03.018>.
682